J Mater Sci (2008) 43:3400–3407
DOI 10.1007/s10853-008-2523-3

Structure and mechanical properties of gradient coatings deposited by PVD technology onto the X40CrMoV5-1 steel substrate

K. Lukaszkowicz · L. A. Dobrzański

Received: 28 June 2007 / Accepted: 31 January 2008 / Published online: 21 February 2008

Abstract This paper presents the research results on the structure and mechanical properties of gradient coatings deposited by PVD methods on the X40CrMoV5-1 steel substrate. The tests were carried out on TiAlN, TiCN and AlSiCrN coatings. It was found that the structure of the PVD coatings consisted of fine crystallites, while their average size fitted within the range of 15–50 nm, depending on the coating type. The coatings demonstrated columnar structure as well as good adherence to the substrate, the latter not only being the effect of adhesion but also by the transition zone between the coating and the substrate, developed as a result of diffusion and high-energy ion action that caused mixing of the elements in the interface zone. The critical load L_{C2} lies within the range of 46–59 N, depending on the coating type. The TiAlN coatings demonstrate the highest hardness and abrasive wear resistance. The good properties of the PVD gradient coatings make them suitable in various engineering and industrial applications.

Introduction

For several decades, tool material designers have been trying to develop and produce an ideal tool material of high ductility and maximum possible wear resistance characteristics in working conditions. Such combination is practically impossible to obtain. Therefore, various attempts were made to find at least a partial solution to the issue, by creation of layer structures, the methods included without limitation of thermal–chemical treatment, composite material production and monolayer coating deposition by the CVD and PVD methods as well as overlaying welding or hard layer spraying by the spray metallization method [1–5]. Each of these methods, however, represents restrictions caused by inappropriate thickness of the surface layer, and, particularly, the issues due to the inappropriate adhesion of the layer produced or the excessive stresses between the surface layer and the substrate. Such stresses often cause accelerated layer spalling or chipping, especially when superposition occurs between the internal structural stresses and external ones caused by loads developed in working conditions.

Gradient coatings deposited on the tool material substrate and providing appropriately high resistance to abrasive wear in tool operating conditions, core ductility and stress relaxation between the particular coating layers and between the gradient coating and tool material coating are seen as a solution to the issue [6–8]. Functional gradient coatings create a new class of coatings with properties and structure changing gradually. Frequently a rapid difference between the coating and substrate properties occurs causing a stress concentration in this area, both during the manufacturing and operation of the tools. This causes fast degradation demonstrated by cracks and delamination of the coatings. The application of functional gradient coatings offers a possible solution to the issue. Gradient coatings can be applied in manufacturing modern machining tools, due to their resistance to high-temperature oxidation and erosion as well as abrasive wear. Two groups can be identified within the range of applications of gradient coatings [9, 10]:

K. Lukaszkowicz (✉) · L. A. Dobrzański
Institute of Engineering Materials and Biomaterials, Silesian University of Technology, Konarskiego St. 18A, 44-100 Gliwice, Poland
e-mail: krzysztof.lukaszkowicz@polsl.pl

- gradient wear-resistant coatings (GWRC),
- gradient thermal barrier coatings (GTBC).

There has been intensive research for almost 15 years now, concerning the preparation and distribution of functional gradient materials. One of the manufacturing methods described in the references is powder metallurgy with properties varying by gradients (from hard on the surface to ductile in the core) [11]. The layers are alloyed, pad welded or fusion penetrated by laser (thanks to the share of very hard phases varying by gradients with their highest concentration on the surface), assuring the highest hardness and wear resistance and the core ductility required thanks to the low content of hard phases in the deeper located gradients. Finally, there are PVD or CVD coatings assuring high wear resistance (GWRC) and thermal barrier (GTBC).

The aim of this paper is to examine the structure and mechanical properties of the gradient coatings deposited by PVD method onto the X40CrMoV5-1 hot work tool steel substrate.

Materials and methods

The examinations have been made on specimens of hot work tool steel X40CrMoV5-1 (56 HRC, 30 × 5 mm) deposited in the PVD process with hard TiAlN, TiCN, AlSiCrN gradient coatings.

Specimens were subjected to heat treatment consisting of quenching and tempering; austenizing was carried out in a vacuum furnace at 1020 °C with a soaking time of 0.5 h. Two isothermal holds were used during heating up to the austenizing temperature, the first at a temperature of 640 °C and the second at 840 °C. The specimens were tempered twice after quenching, each time for 2 h at the temperature of 560 °C and next at 510 °C. To ensure proper quality, the surfaces of the steel specimens were subjected to mechanical grinding and polishing ($R_a = 0.03$ μm).

The coating deposition process was made in a device based on the cathodic arc evaporation (CAE) method. Cathodes containing pure metals (Ti, Cr), the TiAl (50:50 at.%) alloy and the AlSi (88:12 wt.%) alloy were used for deposition of the coatings. The base pressure was 5×10^{-6} mbar, the deposition temperature was approximately 350 °C (in case of the TiCN coatings −500 °C). TiAlN and AlSiCrN gradient coatings were obtained using the variable nitrogen flow rate from 100 to 250 sccm. TiCN gradient coatings were obtained using the variable nitrogen flow rate from 250 to 100 sccm and acetylene from 0 to 200 sccm. The bias voltage was −60 V in all cases. The deposition conditions are summarized in Table 1.

Diffraction and thin film structure were tested with the use of the JEOL JEM 3010UHR transmission electron microscope, at 300-kV bias voltage. The thin films were produced as a result of mechanical thinning and further ionic polishing using the Gatan apparatus.

Observations of surface and structures of the deposited coatings were carried out on cross sections in the SUPRA 25 scanning electron microscope. Detection of secondary electron was used for generation of fracture images with 15-kV bias voltage and 30,000× maximum magnification.

The phase composition of the investigated coatings was determined by means of the DRON-2.0 X-ray diffractometer, using the filtered X-radiation of the cobalt anode lamp, at 40-kV supply voltage and 20-mA glow current intensity.

The chemical concentration changes of the coating components, both perpendicular to their surface and in the transition zone between the coating and the substrate material, were evaluated in tests carried out in the GDOS-750 QDP glow-discharge optical spectrometer from Leco Instruments. The following operation conditions of the spectrometer Grimm lamp were fixed during the tests:

- lamp inner diameter—4 mm;
- lamp supply voltage—700 V;
- lamp current—20 mA;
- working pressure—100 Pa.

A continuous concurrent spectrometer in the Paschen-Runge system was used in this device, with 750-mm focal distance and a holographic mesh with 2400 lines per millimetre.

Tests of the coatings' adhesion to the substrate material were made using the scratch test on the CSEM REVETEST device, by moving the diamond indenter along the

Table 1 Deposition parameters of the coatings

Coating	Substrate bias voltage (V)	Arc current source (A)	Temperature (°C)	Gas mixture	
				Nitrogen flow rate (sccm)	Acetylene flow rate (sccm)
TiAlN	−60	TiAl-60	350	100 → 250	–
AlSiCrN	−60	Cr-60 AlSi-60	350	100 → 250	–
TiCN	−60	Ti-60	500	250 → 100	0 → 200

examined specimen's surface with gradually increasing load. The radius of the diamond indenter used in the scratch test was 200 μm. The device registered the friction force, friction coefficient, indenter penetration depth and acoustic emission along the scratch track. The tests were made using the following parameters:

- load range: 0–100 N,
- load increase rate (dL/dt): 100 N/min,
- indenter's sliding speed (dx/dt): 10 mm/min,
- acoustic emission detector's sensitivity AE: 1.

The critical load L_C, causing the loss of the coating adhesion to the material, was determined on the basis of the values of the acoustic emission AE and friction force F_t recorded and observation of the damage developed in the scratch test on a LEICA MEF4A light microscope.

During the adhesion scratch tests of the coatings the following damage was observed [12, 13]:

- spalling failure,
- buckling failure,
- chipping failure,
- conformal cracking,
- tensile cracking.

The microhardness tests of coatings were made with the SHIMADZU DUH 202 ultra-microhardness tester. The test conditions were selected so as to obtain comparable test results for all coatings. Measurements were made at 0.05 N load, to eliminate the substrate impact on the coating hardness.

The thickness of coatings was determined using the "kalotest" method, i.e. measuring the characteristics of the spherical cap crater developed on the surface of the coated specimen tested.

Results and discussion

The coatings' structure appears to be compact without any visible delamination or defects. The investigated coatings tested show a columnar structure that may be considered compatible with the Thornton model (zone I), except the fact that in TiCN the cross-section morphology is dense (Figs. 1–3). The fractographic tests on the steel specimens covered with the TiAlN and TiCN coatings indicate a sharp interface zone between the substrate and the coatings.

The TiAlN and TiCN coating observations in the TEM (Fig. 4) indicate that such coatings consist of fine crystallites, of average size ca. 15–50 nm, depending on the kind of coating. Generally, there are no foundations to confirm the epitaxial growth of the investigated coatings. Several large grains were observed in the CrAlSiN coating (Fig. 5), and the possibility of epitaxy due to the presence of large

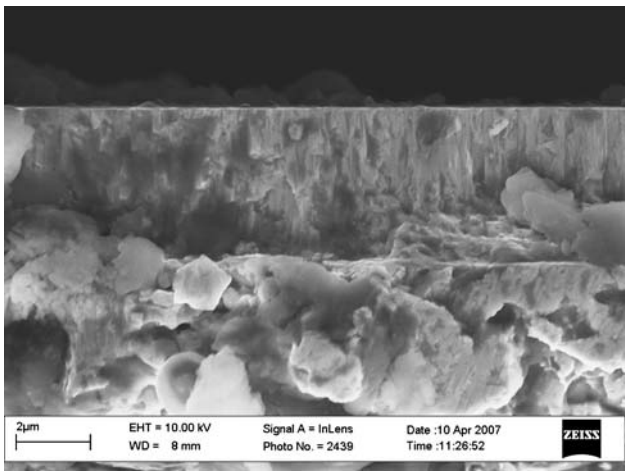

Fig. 1 Fracture of the TiAlN coating deposited onto the X40CrMoV5-1 steel substrate

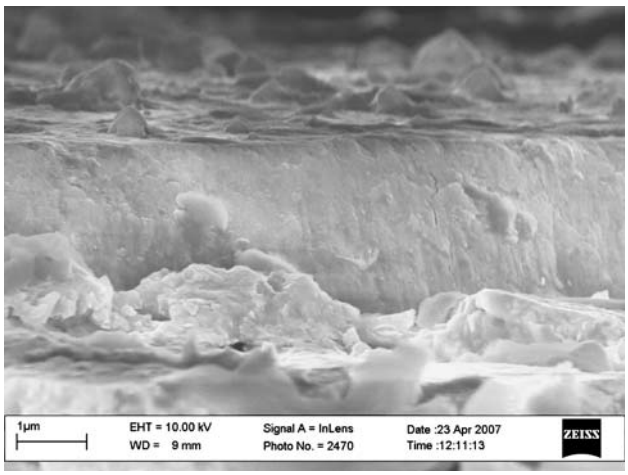

Fig. 2 Fracture of the TiCN coating deposited onto the X40CrMoV5-1 steel substrate

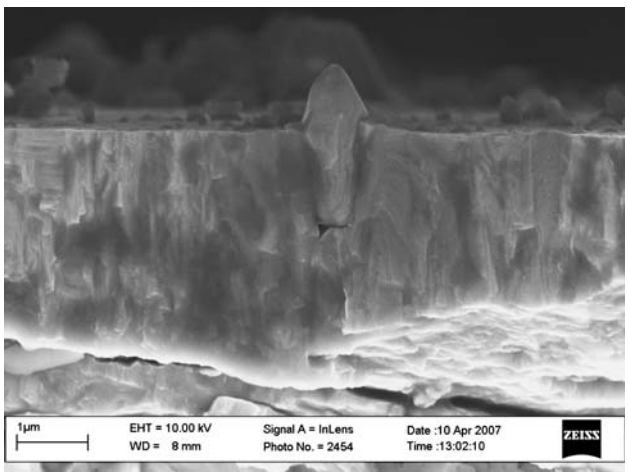

Fig. 3 Fracture of the AlSiCrN coating deposited onto the X40CrMoV5-1 steel substrate

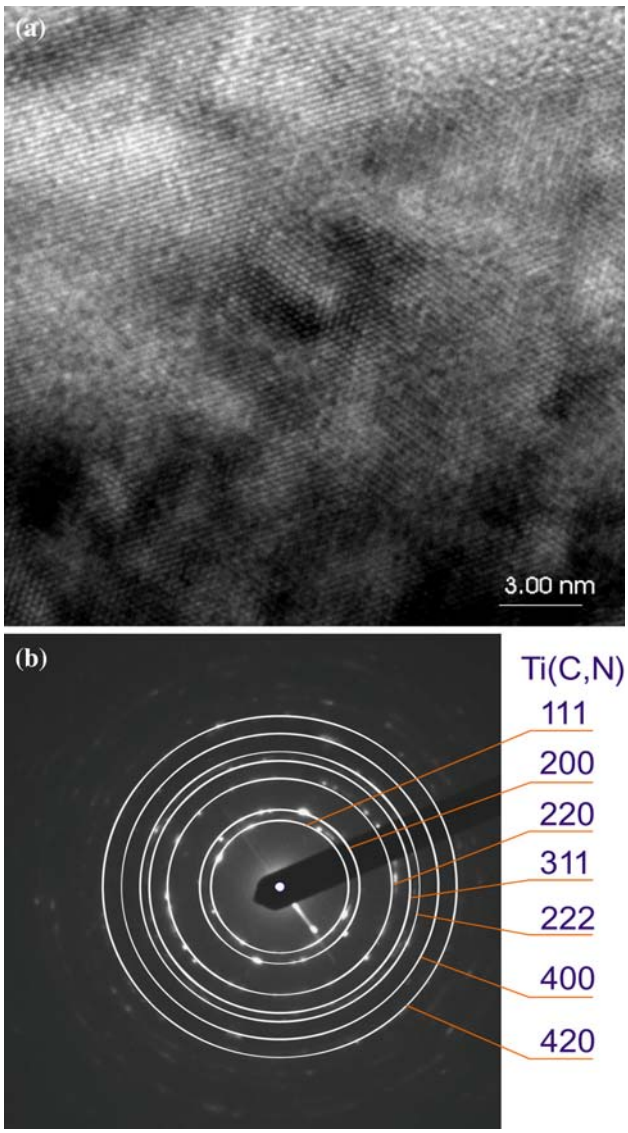

Fig. 4 (**a**) Structure of the thin foil from the TiCN coating deposited onto the hot work tool steel X40CrMoV5-1, (**b**) diffraction pattern from the area as in figure a and solution of the diffraction pattern

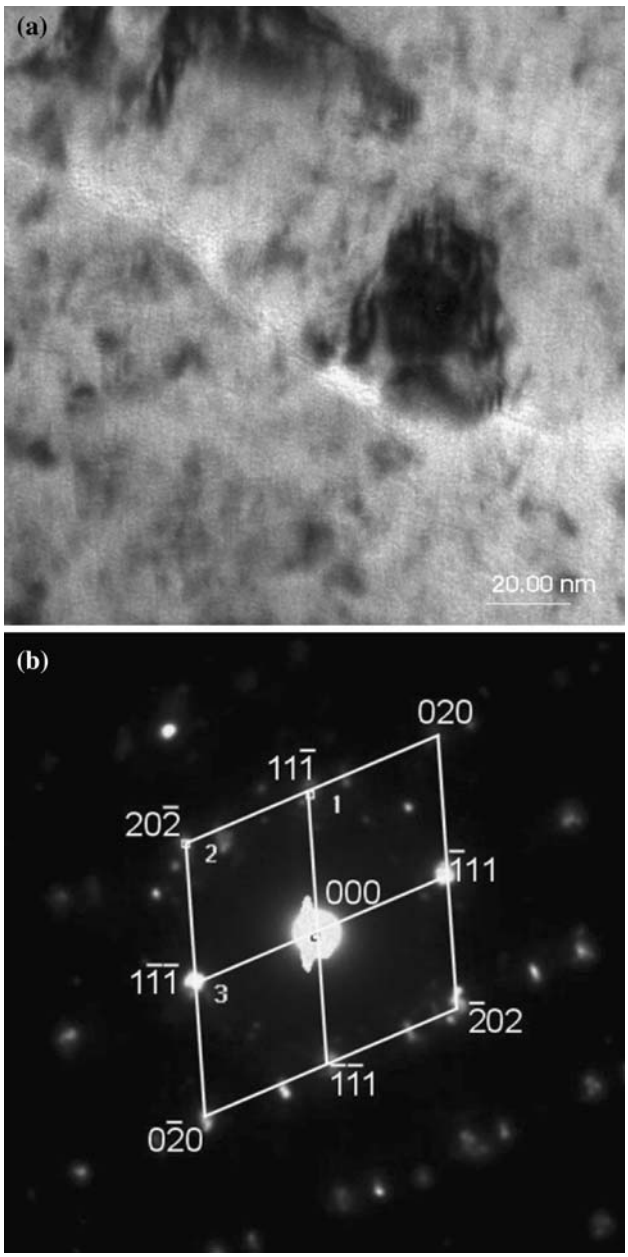

Fig. 5 (**a**) Structure of the thin film of the AlSiCrN coating deposited onto the hot work tool steel X40CrMoV5-1, (**b**) diffraction pattern from the area as in figure a and solution of the diffraction pattern indicating (Cr,Al)N phase

crystallites may be deduced upon examination of the SAED pattern.

X-ray diffraction patterns of the investigated samples (Figs. 6–8) have shown that the coatings contain one fcc phase only. In case of the TiAlN phase the diffraction lines are shifted to the larger deflection angles, compared to the TiN phase diffraction lines. The reduction of the lattice parameter with NaCl structure, typical for TiN from 0.423 nm to 0.418 nm, is the reason, because of substitution of Ti atoms ($r = 0.146$ nm) by Al atoms ($r = 0.143$ nm). The hexagonal AlN phase of a wurtzite-type structure was not detected in the AlSiCrN and TiAlN coatings, which may be due to their low aluminium content.

Figures 9, 10 present the changes of the chemical concentrations of the coating constituents and substrate material upon tests carried out on the glow-discharge optical emission spectroscope.

The GDOS tests also indicate the existence of the transition zone between substrate material and coating, improving adhesion of the deposited coatings to the substrate. In the transition zone the concentration of elements included in the substrate grows, while the concentration of elements constituting the coatings decreases rapidly. Its

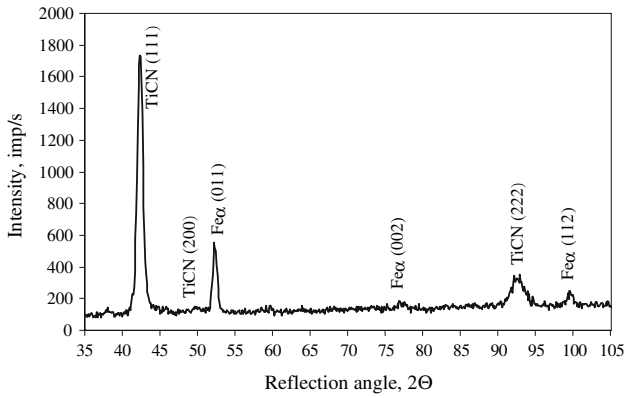

Fig. 6 X-ray diffraction pattern of the TiCN coating deposited onto the hot work tool steel X40CrMoV5-1

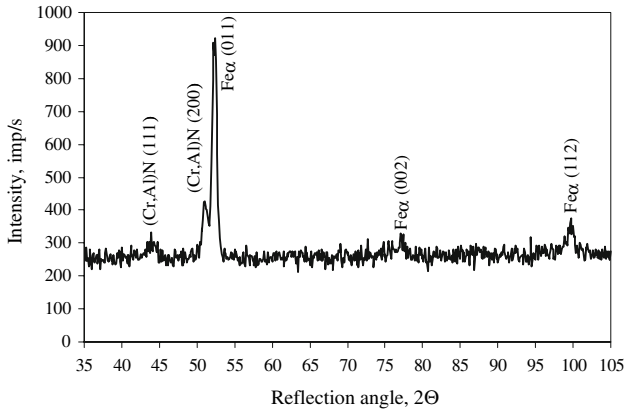

Fig. 7 X-ray diffraction pattern of the AlSiCrN coating deposited onto the hot work tool steel X40CrMoV5-1

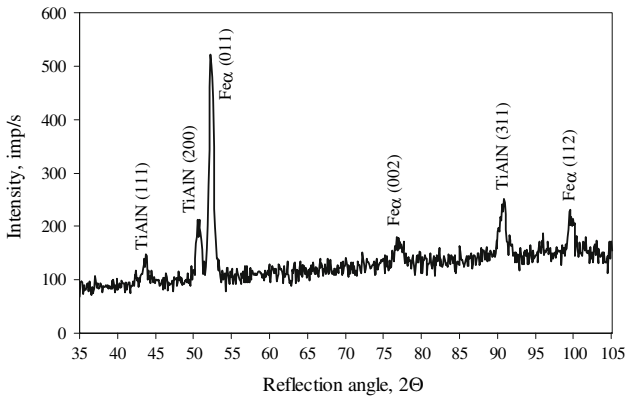

Fig. 8 X-ray diffraction pattern of the TiAlN coating deposited onto the hot work tool steel X40CrMoV5-1

development may also be connected with high-energy ions causing transfer of the elements in the joint zone, increase of desorption of the substrate surface and development of defects in the substrate. It should be emphasized, however, that the results obtained with the use of the GDOS cannot

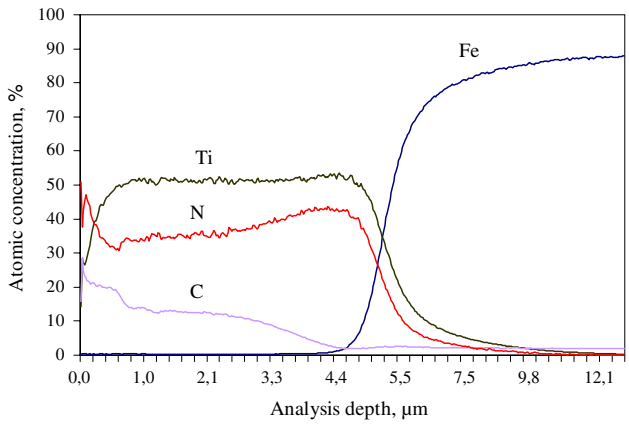

Fig. 9 Changes of constituent concentration of the TiCN and the substrate materials

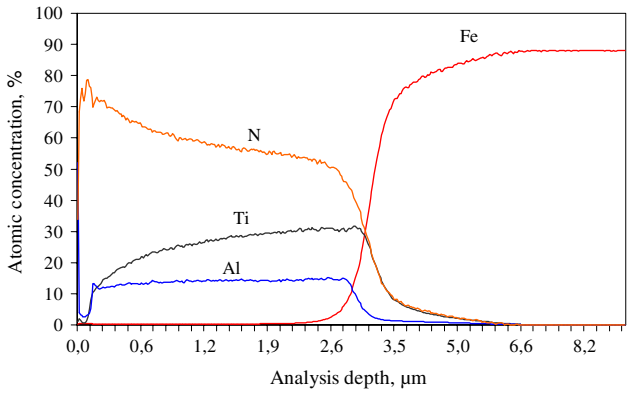

Fig. 10 Changes of constituent concentration of the TiAlN and the substrate materials.

Table 2 The characteristics of the tested coatings

Coating	Thickness (μm)	Critical load L_{C1} (*N*)	Critical load L_{C2} (*N*)	Microhardness (GPa)
TiAlN	2.8 ± 0.1	19 ± 2	46 ± 4	32.8 ± 1.2
AlSiCrN	2.1 ± 0.1	25 ± 2	46 ± 3	32.1 ± 1.4
TiCN	4.2 ± 0.3	28 ± 2	59 ± 4	29.9 ± 0.9

be interpreted unequivocally, due to inhomogeneous vaporization of the specimen material during the tests.

The hardness of the X40CrMoV5-1 steel substrate without coating is 2.1 GPa, as settled upon hardness tests. The deposition of the PVD coatings onto the specimens causes the growth of hardness of the surface layer rainging from 29.9 to 32.8 GPa. The highest hardness, i.e. 32.8 GPa, was noted in the TiAlN coating; while the lowest, i.e. 29.9 GPa, is characteristic for the TiCN coating (Table 2).

The critical loads L_{C1} and L_{C2} were determined in scratch tests. The first critical load L_{C1} corresponds to the

point at which first damage is observed; the first appearance of microcraking, surface flaking outside or inside the track without any exposure of the substrate material—the first cohesion-related failure event (Figs. 11a, 12a, 13a). It has the shape of an interfacial shell-shaped spallation. L_{C1} corresponds to the first small jump on the acoustic emission signal, as well as on the friction force curve (Figs. 14–16). The second critical load L_{C2} is the point at which complete delamination of the coating starts; the first appearance of cracking, chipping, spallation and delamination outside or inside the track with the exposure of the substrate material—the first adhesion-related failure event (Figs. 11b, 12b, 13b). After this point, all the acoustic emission and friction force signals become noisier (Figs. 14–16) [14, 15]. The cumulative test results have been listed and compared in Table 2.

To establish the nature of damage causing the increase of acoustic emission intensity, the examinations of the scratches that arose during the test were made with the use of the light microscope coupled with a measuring device, thus determining the value of the L_C critical load on the basis of metallographical observations. The TiCN coating had the highest critical load of $L_{C1} = 33$ and $L_{C2} = 59$ N, whereas AlSiCrN and the TiAlN coatings had the lowest $L_{C1} = 19$ and $L_{C2} = 46$ N. The TiCN coatings show the best adhesion to the substrate of all the gradient coatings tested, which is not only due to the adhesion itself, but also due to mixing of the elements in the transition zone between the coating and the substrate as a result of diffusion, because the TiCN coatings' deposition process temperature was 500 °C.

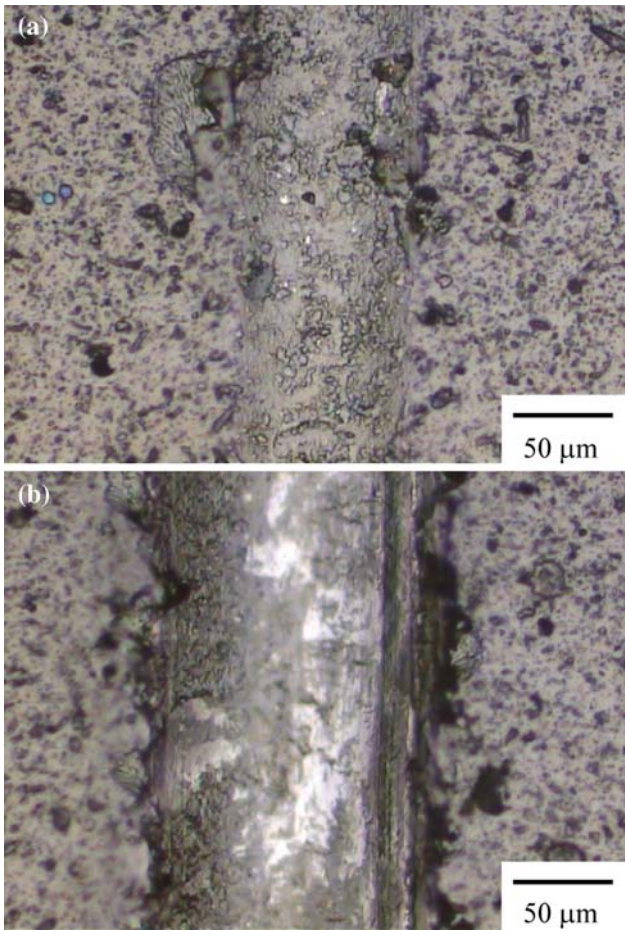

Fig. 11 Scratch failure pictures of the gradient AlSiCrN coating on X40CrMoV5-1 steel substrate at: (**a**) L_{C1}, (**b**) L_{C2}

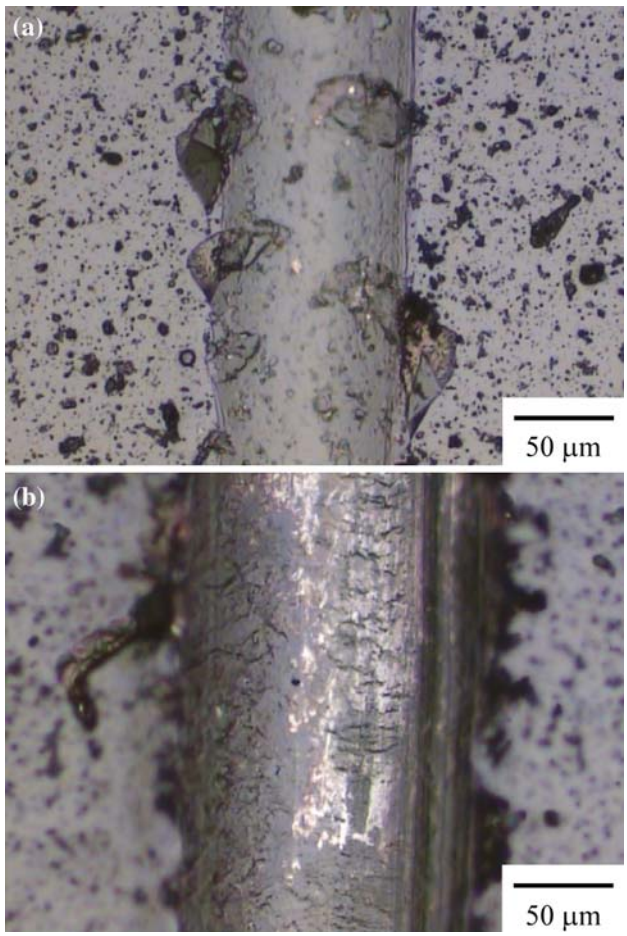

Fig. 12 Scratch failure pictures of the gradient TiAlN coating on X40CrMoV5-1 steel substrate at: (**a**) L_{C1}, (**b**) L_{C2}

Summary

The compact structure of the coatings without any visible delamination was observed in the scanning electron microscope. The investigated TiAlN and CrAlSiN coatings show columnar structure, which may be considered compatible with the Thornton model (zone I). Upon examination of the thin films obtained from TiAlN and

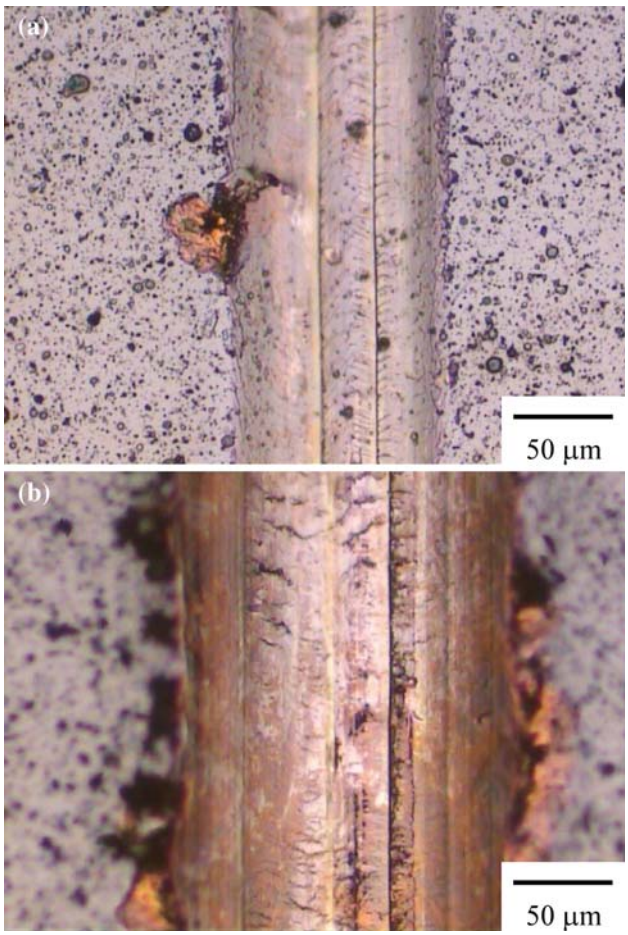

Fig. 13 Scratch failure pictures of the gradient TiCN coating on X40CrMoV5-1 steel substrate at: (**a**) L_{C1}, (**b**) L_{C2}

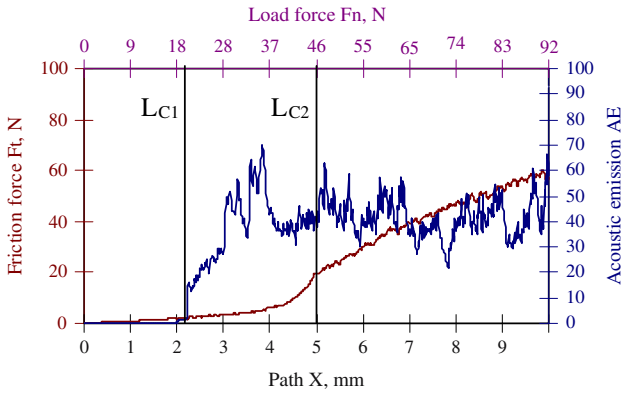

Fig. 14 Diagram indicating the dependence of the acoustic emission (AE) and friction force F_t on the load for the X40CrMoV5-1 steel with the gradient AlSiCrN coating

TiCN coatings, it was found that the coatings were composed of fine crystallites.

The scratch tests on coating adhesion reveal the cohesive and adhesive properties of the coatings deposited on

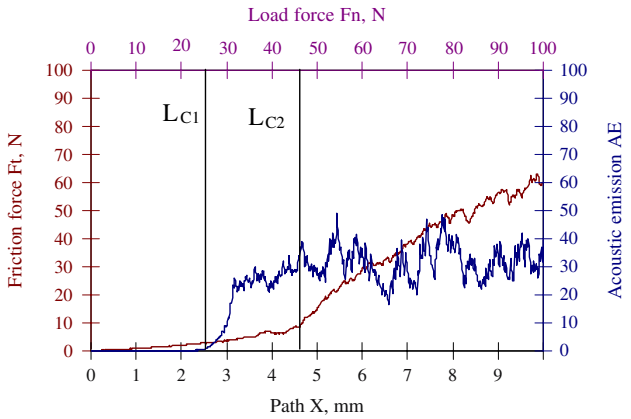

Fig. 15 Diagram of the dependence of the acoustic emission (AE) and friction force F_t on the load for the X40CrMoV5-1 steel with the gradient TiAlN coating

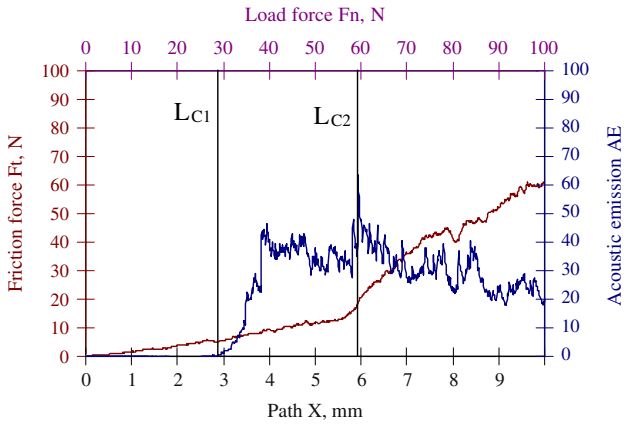

Fig. 16 Diagram of the dependence of the acoustic emission (AE) and friction force F_t on the load for the X40CrMoV5-1 steel with the gradient TiCN coating

the substrate of the X40CrMoV5-1 hot work tool steel. On the basis of the above examinations, it was found that the critical load of L_{C2} is between 46 and 59 N. The highest value of the critical load was obtained for the TiCN coating. The GDOS investigations indicate the existence of the transition zone between the substrate material and the coating resulting in the improved adhesion of the coatings deposited on the substrate.

References

1. Dobrzanski LA, Mazurkiewicz J, Hhajduczej E (2004) J Mater Process Technol 157–158:472
2. Dobrzanski LA, Matula G, Varez A, Levenfeld B, Torralba JM (2004) J Mater Process Technol 157–158:658
3. Klimpel A, Janicki D, Klimpel AS, Rzeznikiewicz A (2007) J Achieve Mater Manuf Eng 20:37
4. Karpov LP (2003) Met Sci Heat Treat 45:8

5. Dobrzanski LA, Lukaszkowicz K (2004) J Mater Process Technol 157–158:317
6. Voevodin AA, Zabinski JS, Muratore C (2005) Tsinghua Sci Technol 10:665
7. Dahan I, Admon U, Frage N, Sariel J, Dariel MP, Moore JJ (2001) Surf Coat Technol 137:111
8. Ssculz U, Peters M, Bach FW, Tegeder G (2003) Mater Sci Eng 362:61
9. Movchan BA, Marinski GS (1998) Surf Coat Technol 100–101:309
10. Guo H, Bi X, Gong S, Xu H (2001) Scripta Materialia 44:683
11. Dobrzanski A, Matula G, Herranz G, Varez A, Levenfeld B, Torralba JM (2006) J Mater Process Technol 175:173
12. Burnett PJ, Rickerby DS (1987) Thin Solid Films 154:403
13. Bellido-Gonzalez V, Stefnopoulos N, Deguilhen F (1995) Surf Coat Technol 74–75:884
14. Sergici AO, Randall NX (2006) Adv Mat Process 4:1
15. He Y, Apachitei I, Zhou J, Walstock T, Duszczyk J (2006) Surf Coat Technol 201:2534